

# A Comparative Study for Molecular Dynamics Simulations of Liquid Benzene

Cen-Feng Fu and Shan Xi Tian\*

Hefei National Laboratory for Physical Sciences at the Microscale and Department of Chemical Physics, University of Science and Technology of China, Hefei, Anhui 230026, China

**ABSTRACT:** The classical equilibrium and nonequilibrium molecular dynamics simulations for liquid benzene, the prototypical aromatic  $\pi-\pi$  interaction system, are performed using a variety of molecular force fields, OPT-FF, AMBER 03, general AMBER force field (GAFF), OPLS-AA, OPLS-CS, CHARMM27, GROMOS 53A5, and GROMOS 53A6. The simulated results of the molecular structure and thermodynamic properties of liquid benzene are compared with the experimental data available in the literature, accounting for the superiority of each force field in the descriptions of the  $\pi-\pi$  interaction system. The OPLS-AA force field is recommended to be the best one, which reproduces quite well the properties examined in this work, while the others fail in predicting either the local structure or the thermodynamic properties. Such distinct discrepancies for the above force fields are discussed within the scheme of the pairwise interaction construction of the standard force field, which will stimulate searching for a force field with generally good quality not only in terms of microstructure descriptions but also in the predictions of the thermodynamic properties of the liquids.

## 1. INTRODUCTION

Interaction between  $\pi$ -aromatic molecules attracts great interest, owing to its crucial significance in the multidisciplinary fields such as DNA base stacking,<sup>1</sup> protein folding and structure,<sup>2–5</sup> drug design,<sup>6,7</sup> stereochemistry of organic reactions,<sup>8</sup> molecular recognitions, host–guest chemistry, and crystal packing.<sup>9–16</sup> In theoretical studies of complex large systems, the classical molecular dynamics (MD) and Monte Carlo (MC) simulations are frequently applied, owing to their high computational efficiencies. It is of the utmost importance to establish a procedure for qualifying the force field for weak intermolecular interactions, in particular,  $\pi-\pi$  interactions of DNA and proteins.<sup>1–5</sup> Molecular clusters consisting of benzene (the typical  $\pi$ -aromatic molecule) have been studied extensively to reveal effects of the intermolecular aromatic  $\pi-\pi$  interactions on the cluster structures and physicochemical properties. As for the benzene dimer in the gas phase, a lot of experimental<sup>17–25</sup> and theoretical<sup>26–34</sup> studies on the stability of different configurations have been reported. What is more, the larger benzene clusters, e.g., trimer, tetramer, and so on, were also investigated to give a detailed description of the aromatic  $\pi-\pi$  interactions in the cluster.<sup>19–21,35–37</sup> Nevertheless, the essential demand toward an understanding of  $\pi$ -aromatic interactions in condensed matter calls on us to explore the structure of aromatic molecule liquids. Consequently, liquid benzene, as the prototypical case, has been studied by X-ray diffraction,<sup>38</sup> neutron diffraction,<sup>39–41</sup> and molecular simulations.<sup>42–50</sup>

High-level quantum chemistry methods, such as the coupled-cluster singles, doubles, and perturbative triples [CCSD(T)] method and density-functional-theory- (DFT-)based symmetry-adapted perturbation method, were employed in the studies of the benzene dimer in the gas phase.<sup>27–34</sup> The parallel displaced (PD) and T-shaped (T; see Figure 1) configurations were found to be nearly isoenergetic, in which the T configuration has been experimentally confirmed as the global energy minimum.<sup>22–25</sup> The computationally inexpensive DFT with improvements to the deficiency in the previous exchange-correlation functionals<sup>51–56</sup> also can provide an

accurate description of the weak  $\pi-\pi$  interactions. In the classical MD and MC studies of the aromatic molecule systems, the results are heavily dependent on the force fields used in the simulations. At least, the selected force fields must be able to reproduce the intermolecular  $\pi-\pi$  interaction potentials. Although many MD and MC studies on liquid benzene using the different force fields have been reported,<sup>42–50</sup> there is no conclusive answer to which field force could be the best to reproduce both the liquid structure and the thermodynamic properties. Recently, Headen et al.<sup>41</sup> obtained a full six-dimensional spatial and orientational picture of liquid benzene by means of high-resolution neutron diffraction and empirical potential structure refinement simulations. They concluded that the first neighbor shell, containing approximately 12 molecules, appears nearly isotropic; at the small molecular separation ( $<0.50$  nm), the favored nearest neighbor geometry is the PD configuration, while at a larger molecular separation ( $>0.50$  nm), the perpendicular Y-shaped configuration (Y; see Figure 1) is predominant.<sup>41</sup> The T configuration, proposed as the global minimum for the gas-phase benzene dimer, occurs only as a saddle point in the liquid state.<sup>41</sup> The force fields used in the MD simulations for liquid benzene become extremely sensitive, namely, the questions of whether they could reproduce the slightly different interaction energies (deviations less than 1 kcal/mol)<sup>33,34</sup> of four dimer configurations, S (sandwich), PD, T, and Y depicted in Figure 1, and whether the subtle energetic differences of these configurations influence the structure and thermodynamic properties of liquid benzene. Therefore, it is deserving to carry out a comprehensive MD simulation study of liquid benzene with the different force fields, more importantly, evaluating the qualities of these force fields.

Up to date, there are many popular force fields used for protein, DNA, and small organic molecule systems, in particular, widely applicable and recent modified force fields such as

Received: March 28, 2011

Published: June 06, 2011

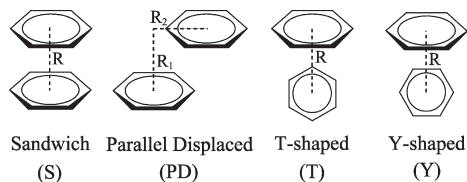


**Figure 1.** Sandwich (S), parallel displaced (PD), T-shaped, and Y-shaped configurations of benzene dimer.

AMBER 03,<sup>57</sup> general AMBER force field (GAFF),<sup>58</sup> OPLS-AA,<sup>59,60</sup> CHARMM27,<sup>61,62</sup> and GROMOS 53A5 and GROMOS 53A6.<sup>63</sup> More recently, Baker and Grant<sup>49</sup> developed a charge-separated all-atom force field, OPLS-CS (originated from OPLS-AA force field<sup>43</sup>), for liquid benzene, on the basis of Hunter and Sanders<sup>64</sup> conclusion that molecular mechanics calculations without the spatial charge distribution of the  $\pi$ -electron system are unlikely to be successful in modeling aromatic system. Additionally, the symmetry-adapted perturbation theory (SAPT) analysis of the benzene dimer shows that the induction terms should be a relatively minor contribution to the noncovalent interactions involving  $\pi$ -aromatic systems, and the predominant factors are electrostatics, exchange-repulsion, and dispersion.<sup>29,31,32,34</sup> This suggests that the standard force fields with point-charge electrostatics may be competent in predicting reliable results for such interactions. Hence, Sherrill et al.<sup>65</sup> recently derived a standard force field OPT-FF by fitting high-level *ab initio* potential curves of the benzene dimer. In the present work, eight sets of the standard force fields, OPT-FF,<sup>65</sup> AMBER 03,<sup>57</sup> GAFF,<sup>58</sup> OPLS-AA,<sup>43</sup> OPLS-CS,<sup>49</sup> CHARMM27,<sup>61,62</sup> GROMOS 53A5,<sup>63</sup> and GROMOS 53A6,<sup>63</sup> are used in the MD simulation study of liquid benzene properties, including its long-range structure, the local structure, and thermodynamic properties. The simulation results will be compared with the experimental data available in the literature, aiming at evaluating the superiority of these force fields for the  $\pi$ -aromatic system.

## 2. COMPUTATIONAL METHODS

**2.1. Benzene Force Fields.** For the all-atom force fields used here, OPT-FF,<sup>65</sup> AMBER 03,<sup>57</sup> GAFF,<sup>58</sup> OPLS-AA,<sup>43</sup> OPLS-CS,<sup>49</sup> CHARMM27,<sup>61,62,66</sup> GROMOS 53A5,<sup>63</sup> and GROMOS 53A6,<sup>63</sup> their intermolecular nonbonding interactions were described by the Lennard-Jones plus Coulomb potential:

$$U(r_{ij}) = 4\epsilon_{ij} \left[ \left( \frac{\sigma_{ij}}{r_{ij}} \right)^{12} - \left( \frac{\sigma_{ij}}{r_{ij}} \right)^6 \right] + \frac{q_i q_j}{4\pi\epsilon_0 r_{ij}} \quad (1)$$

In the OPT-FF, AMBER 03, GAFF, and CHARMM27 force fields, the parameters  $\epsilon_{ij}$  and  $\sigma_{ij}$  were calculated following the rules as  $\epsilon_{ij} = (\epsilon_i \epsilon_j)^{1/2}$  and  $\sigma_{ij} = (\sigma_i + \sigma_j)/2$ , while for the OPLS-AA, OPLS-CS, GROMOS 53A5, and GROMOS 53A6 force fields, the parameters  $\epsilon_{ij}$  and  $\sigma_{ij}$  were calculated following the rules as  $\epsilon_{ij} = (\epsilon_i \epsilon_j)^{1/2}$  and  $\sigma_{ij} = (\sigma_i \sigma_j)^{1/2}$ . The parameters of these force fields are listed in Table 1. The parameters of the GAFF force field were generated by ANTECHAMBER.<sup>67</sup> The effective charges of the GAFF force field were obtained by fitting the quantum-chemistry derived gas-phase electrostatic potentials with the restrained electrostatic potential (RESP) method.<sup>68</sup> As described in ref 58, both geometry optimization

and single-point calculation were reperformed at the HF/6-31G\* level in this work. For the AMBER 03 force field, the effective charges were also obtained by fitting the electrostatic potential with the RESP method.<sup>68</sup> Here, it is noted that, as described in ref 57, the geometry optimizations were done at the RHF/6-31G\*\* level. Subsequently, the IEFPCM continuum solvent model was used to reproduce an organic solvent environment ( $\epsilon = 4$ ), and a single-point calculation at the B3LYP/cc-pVTZ level was performed to obtain the electrostatic potential. These quantum chemistry calculations were carried out with the Gaussian 03 suite of programs.<sup>69</sup>

**2.2. Equilibrium MD Simulations.** All of the classical MD simulations were performed with the GROMACS program package.<sup>70,71</sup> Initially, the system containing 600 benzene molecules was generated in a cubic box ( $89.0511 \text{ nm}^3$ ) with the density equal to the experimental value ( $873.8 \text{ kg/m}^3$ ).<sup>72</sup> The periodic boundary condition was implemented. The system was energy-minimized for the first 5000 steps using the conjugate gradient method with one additional steepest descent step following every conjugate gradient step. Subsequently, a 10.0 ns MD simulation in the NPT ensemble was performed at  $P = 1 \text{ atm}$  and  $T = 298 \text{ K}$  with a 1 fs step to equalize the system. Finally, a 10.0 ns MD simulation in the NPT ensemble was carried out at  $P = 1 \text{ atm}$  and  $T = 298 \text{ K}$  with a 1 fs step for the product collecting simulation. The Nosé–Hoover thermostat<sup>73,74</sup> with a coupling time of 0.5 ps was employed to regulate the temperature. The Parrinello–Rahman isotropic barostat<sup>75,76</sup> was used to impose constant pressure with a 2.0 ps coupling time. The cutoff distance for van der Waals interactions was 1.5 nm, with a long-range dispersion correction applied for energy. The particle-mesh Ewald (PME) method<sup>77</sup> was employed to treat Coulomb interactions, using a 1.3 nm cutoff for real-space, a grid spacing of 0.12 nm, and a PME order of 8. All bonds were constrained using the P-LINCS algorithm.<sup>78,79</sup>

The calculations of heat capacity at constant pressure ( $C_p(l)$ ) and vaporization enthalpy ( $\Delta H_{\text{vap}}$ ) are performed in the usual way.<sup>44</sup> The intermolecular component  $C_p^{\text{inter}}(l)$  of  $C_p(l)$  is estimated from the fluctuation of intermolecular energy  $E_{\text{inter}}$ :

$$C_p^{\text{inter}}(l) = \frac{\langle (E_{\text{inter}} + PV)^2 \rangle - \langle E_{\text{inter}} + PV \rangle^2}{N_A k_B T^2} \quad (2)$$

where  $N_A$  is Avogadro's constant and  $k_B$  is the Boltzmann constant.  $C_p(l)$  is further calculated with

$$C_p(l) = C_p^{\text{inter}}(l) + C_p^{\circ}(g) - R \quad (3)$$

where the heat capacity of the ideal gas  $C_p^{\circ}(g)$  is  $19.5 \text{ cal mol}^{-1} \text{ K}^{-1}$  at  $298 \text{ K}$ ,<sup>44</sup>  $R$  is the gas constant, and the  $g$  in parentheses represents the gas phase.  $\Delta H_{\text{vap}}$  is defined as

$$\Delta H_{\text{vap}} = E_{\text{intra}}(g) - (E_{\text{inter}}(l) + E_{\text{intra}}(l)) + RT \quad (4)$$

where  $E_{\text{intra}}$  is the intramolecular energy. Assuming  $E_{\text{intra}}(l) \approx E_{\text{intra}}(g)$ , the above formula can be approximated to be  $\Delta H_{\text{vap}} \approx -E_{\text{inter}}(l) + RT$ .

The self-diffusion coefficients are determined by the Einstein relation<sup>80</sup>

$$D = \lim_{t \rightarrow \infty} \frac{1}{6t} \langle |\mathbf{r}(t) - \mathbf{r}(0)|^2 \rangle \quad (5)$$

where  $\mathbf{r}(t)$  is the center of mass vector position of each molecule at time  $t$ ,  $\mathbf{r}(0)$  is the position at  $t = 0$ , and  $D$  is the self-diffusion coefficient.

**Table 1.** Force Field Parameters for Benzene Used in This Work

parameter	OPT-FF <sup>65</sup>	AMBER 03 <sup>57</sup>	GAFF <sup>58</sup>	OPLS-AA <sup>43</sup>	OPLS-CS <sup>49</sup>	CHARMM27 <sup>61,62</sup>	GROMOS 53AS <sup>63</sup>	GROMOS 53A6 <sup>63</sup>
$R_{CC}$ (Å)	1.40	1.40	1.387	1.40	1.40	1.375	1.39	1.39
$R_{CH}$ (Å)	1.08	1.08	1.087	1.08	1.08	1.080	1.09	1.09
$R_{C\pi}$ (Å)					0.90			
$\theta_{CCC}$ (deg)	120.0	120.0	120.0	120.0	120.0	120.0	120.0	120.0
$\theta_{CCH}$ (deg)	120.0	120.0	120.0	120.0	120.0	120.0	120.0	120.0
$\theta_{CC\pi}$ (deg)					90.0			
$\Psi_{CCCC}$ (deg)	0.0	0.0	0.0	0.0	0.0	0.0	0.0	0.0
$\Psi_{CCCH}$ (deg)	180.0	180.0	180.0	180.0	180.0	180.0	180.0	180.0
$\Psi_{CC\pi}$ (deg)					90.0/-90.0			
$q_C$ ( $\epsilon$ )	-0.134	-0.121866 <sup>a</sup>	-0.130889 <sup>b</sup>	-0.115	0.1435	-0.115	-0.146	-0.140
$q_H$ ( $\epsilon$ )	0.134	0.121866 <sup>a</sup>	0.130889 <sup>b</sup>	0.115	0.1435	0.115	0.146	0.140
$q_\pi$ ( $\epsilon$ )					-0.1435			
$\sigma_C$ (Å)	3.42462	3.39967	3.39967	3.55	3.69	3.55005	3.58118	3.58118
$\sigma_H$ (Å)	2.19161	2.59964	2.59964	2.42	2.52	2.42004	2.37341	2.37341
$\varepsilon_C$ (kcal/mol)	0.115	0.086	0.086	0.07	0.07	0.07	0.06630	0.06630
$\varepsilon_H$ (kcal/mol)	0.011	0.015	0.015	0.03	0.03	0.03	0.02829	0.02829

<sup>a</sup> RESP charges obtained at the B3LYP/cc-pVTZ//RHF/6-31G\*\* level.<sup>b</sup> RESP charges obtained at the HF/6-31G\*//HF/6-31G\* level.

The reorientational dynamics of the liquid were also analyzed. The rotational correlation times ( $\tau$ ) were computed as described by Bonnaud et al.<sup>50</sup> The rotational correlation times are divided into two cases,  $\tau_{2\perp}$  and  $\tau_{2\parallel}$ , that correspond to the relaxation times of the unitary vectors perpendicular  $\hat{\mathbf{e}}_\perp$  and parallel  $\hat{\mathbf{e}}_\parallel$  to the plane of the benzene molecule, respectively (see Figure 2 in ref 50). Two rotational autocorrelation functions can be defined as

$$C_i^l(t) = \langle P_l(\hat{\mathbf{e}}_i(t) \cdot \hat{\mathbf{e}}_i(0)) \rangle \quad (6)$$

where  $\hat{\mathbf{e}}_i$  is  $\hat{\mathbf{e}}_\perp$  or  $\hat{\mathbf{e}}_\parallel$  as defined above and  $P_l$  is a Legendre polynomial with  $l = 1$  an 2 for the first and second orders, respectively. Then, these functions are fitted in the format of the Kohlrausch–Williams–Watts exponential function:<sup>81,82</sup>

$$C_{i,\text{KWW}}^l(t) = \exp[-(t/\alpha_{li})^{\beta_{li}}] \quad (7)$$

where  $0 < \beta_{li} \leq 1$ . After fitting, the rotational correlation time can be obtained as

$$\tau_{il} = \int_0^\infty C_{i,\text{KWW}}^l(t) dt = \frac{\alpha_{lm}}{\beta_{lm}} \Gamma\left(\frac{1}{\beta_{lm}}\right) \quad (8)$$

**2.3. Nonequilibrium MD Simulations.** Nonequilibrium MD simulations were performed to determine the shear viscosity ( $\eta$ ) of liquid benzene. A spatially periodic forcing function is imposed on the system, and the shear viscosity can be determined from the response of the system to the applied function. The behavior of the velocity  $\mathbf{u}(\mathbf{r}, t)$  of a particle in the liquid is described by the Navier–Stokes equation:<sup>83</sup>

$$\rho \frac{\partial \mathbf{u}}{\partial t} + \rho(\mathbf{u} \cdot \nabla) \mathbf{u} = \rho \mathbf{a} - \nabla p + \eta \nabla^2 \mathbf{u} \quad (9)$$

where  $\mathbf{a}$  is the external force per unit of mass and volume and  $\rho$  is the fluid density. A periodic external force  $\mathbf{a}$  is used in cosine form

$$a_x(z) = A \cos(kz) \quad (10)$$

where  $A$  is the applied acceleration,  $l_z$  is the length of the simulation box along the  $z$  direction, and  $k = 2\pi/l_z$ . The

steady-state velocity profile is in the following form by integrating the Navier–Stokes equation:

$$u_x(z) = V(1 - e^{-t/\tau_r}) \cos(kz) \quad (11)$$

$$V = A\tau_r = A \frac{\rho}{\eta k^2} \quad (12)$$

where  $\tau_r$  is the macroscopic relaxation time of the liquid. In an MD simulation, the instantaneous  $V(t)$  is defined as

$$V(t) = 2 \sum_{i=1}^N m_i v_{i,x}(t) \cos(kr_{i,z}(t)) / \sum_{i=1}^N m_i \quad (13)$$

where  $v_{i,x}$  is the  $x$  component of the velocity,  $r_{i,z}$  is the  $z$  coordinate, and  $m_i$  is the mass of atom  $i$ . Then, the viscosity  $\eta$  can be obtained from eq 14 by calculating  $V$  directly from the simulations:

$$\eta = \frac{A\rho}{V k^2} \quad (14)$$

In the nonequilibrium MD simulations, the initial configurations were generated at the equilibrated density for each force field. As mentioned by Hess,<sup>83</sup> the wavelength of the imposed acceleration should be at least an order of magnitude larger than the simulation box; three boxes were stacked in the  $z$  direction, making the system 2 times larger than that used in the equilibrium MD simulations. Wensink et al.<sup>84</sup> concluded that the shear viscosity calculated from the nonequilibrium MD simulation in the *NVT* ensemble was consistent with that calculated in the *NPT* ensemble. Thus, a 5.0 ns simulation for each force field was performed in the *NVT* ensemble. An acceleration of 0.01 nm/ps<sup>2</sup> was imposed on each atom of the system in the  $x$  direction. The temperature was coupled to 298 K, using a Berendsen<sup>85</sup> thermostat with a coupling time of 0.1 ps. The treatments of van der Waals and Coulomb interactions were identical to that for the equilibrium MD simulations. In the simulation analyses, the first 500 ps for each simulation were dropped.

**Table 2.** Equilibrium Energy and Distance of the Different Configurations of the Benzene Dimer

	sandwich (S)		parallel displaced (PD)		T-shaped		Y-shaped		
	E (kcal/mol)	R (Å)	E (kcal/mol)	R <sub>1</sub> (Å)	R <sub>2</sub> (Å)	E (kcal/mol)	R (Å)	E (kcal/mol)	R (Å)
OPT-FF	-1.95	3.70	-2.48	3.50	2.50	-2.92	4.90	-2.90	4.84
AMBER 03	-1.74	3.64	-2.23	3.50	2.40	-2.09	5.10	-2.18	5.00
GAFF	-1.48	3.68	-2.18	3.50	2.66	-2.19	5.10	-2.26	5.00
OPLS-AA	-1.69	3.78	-2.10	3.50	2.68	-2.15	5.10	-2.24	5.02
OPLS-CS	<sup>a</sup>	<sup>a</sup>	-2.89	3.50	4.00	-3.77	5.14	-3.99	5.02
CHARMM27	-1.83	3.76	-2.22	3.50	2.62	-2.11	5.14	-2.23	5.04
GROMOS 53A5	-0.72	3.94	-1.95	3.50	3.34	-2.44	5.06	-2.43	4.98
GROMOS 53A6	-0.88	3.90	-1.94	3.50	3.28	-2.37	5.08	-2.37	4.98
estd. CCSD(T)/CBS( $\Delta h_{\text{a}}(\text{DT})Z$ ) <sup>b</sup>	-1.70	3.9	-2.71	3.5	1.7	-2.70	5.0		
DFT-SAPT/aug-cc-pVTZ+mb <sup>c</sup>	-1.782	3.816	-2.683	3.480	1.841	-2.698	4.970	-2.441	5.009

<sup>a</sup> The sandwich conformation predicted with the OPLS-CS force field is a repulsive state. <sup>b</sup> Cited from ref 33. <sup>c</sup> Cited from ref 34.

### 3. RESULTS AND DISCUSSION

**3.1. Equilibrium Configurations of Benzene Dimer.** The interaction energy of the benzene dimer in the gas phase may give a basis to evaluate the different force fields used in the present MD simulations. As listed in Table 2, the interaction energies of benzene dimers in the different configurations are calculated with the force fields and compared to the high-level quantum chemistry results.<sup>33,34</sup> The equilibrium distances, R, R<sub>1</sub>, and R<sub>2</sub>, are defined in Figure 1. For the S configuration, the interaction energies predicted with the OPT-FF, AMBER 03, OPLS-AA, and CHARMM27 force fields are close to the high-level quantum chemistry results,<sup>33,34</sup> with the percent deviations less than 15%. For the GROMOS 53A5 and GROMOS 53A6 force fields, the equilibrium interaction energies are much lower than the high-level quantum chemistry results.<sup>33,34</sup> It is worth noting that the OPLS-CS force field predicts a repulsive state for the S configuration, due to the separated charges out of the molecular plane that were used to represent the  $\pi$  electrons.<sup>49</sup> As for the PD configuration, the interaction energies predicted with the OPT-FF and OPLS-CS force fields are consistent with the high-level quantum chemistry results,<sup>33,34</sup> with about 9% and 7% deviations, respectively. However, the equilibrium distance R<sub>2</sub> for the OPLS-CS force field is too large, again due to the separated charges used in its potential function. The AMBER 03, GAFF, OPLS-AA, and CHARMM27 force fields are quite good at the prediction of the interaction energies, while a little worse for the GROMOS 53A5 and GROMOS 53A6 force fields. The interaction energy and R value for the T configuration predicted with the OPT-FF force field are in excellent agreement with the quantum chemical results,<sup>33,34</sup> while the others, except for OPLS-CS, underestimate the interaction energy but overestimate the equilibrium distance R, with respect to the high-level quantum chemistry results.<sup>33,34</sup> It is more remarkable that an overestimated energy with about 40% percent deviation is given with the OPLS-CS force field. Regarding to the Y configuration, within 1% and 3% deviations, respectively, the GROMOS 53A5 and GROMOS 53A6 force fields give perfect estimations in comparison with the DFT-SAPT results.<sup>34</sup> The interaction energies predicted with the AMBER 03, GAFF, OPLS-AA, and CHARMM27 force fields are lower with values of 0.2–0.3 kcal/mol, but those for the OPT-FF and OPLS-CS force fields are quite larger (their percent deviations are 19% and 63%, respectively).

Generally, the results of the four configurations of the benzene dimer predicted with the AMBER 03, GAFF, OPLS-AA, and CHARMM27 force fields are comparable to each other and acceptable in comparison with the high-level quantum chemical results.<sup>33,34</sup> Before going on to the details about the effects of such differences on the structural and thermodynamic properties of liquid benzene, we should recall the original characteristics of some force fields. The standard molecular force fields are usually obtained by fitting the *ab initio* pairwise interaction potential energies, while some of them also were adjusted according to the experimental thermodynamic properties of liquids, e.g., OPLS.<sup>43</sup> To qualify the OPLS performances, Jorgensen et al. carried out an MC simulation study of liquid benzene and benzene derivatives, indicating the reliability in thermodynamics predictions.<sup>44</sup> Considering the quadrupole–quadrupole interactions arising from the aromatic  $\pi$  electrons of two benzene molecules, the OPLS parameters were further modified to be OPLS-CS.<sup>49</sup> On the other hand, the CHARMM, AMBER, OPLS-AA, and MM3 force fields were examined in a comparison of the intermolecular interaction potentials of the benzene dimer.<sup>65</sup> In that work, the OPT-FF force field used here was obtained with a much better fitness to the *ab initio* results.<sup>65</sup> However, as pointed out by those authors, the fitted Lennard-Jones parameters hardly reproduce the *ab initio* potentials for four typical configurations of the benzene dimer, and the more flexible electrostatic force fields and the polarization terms should be considered.<sup>65</sup> The computational demand will be enhanced for the sophisticated force fields including complex parameters. It is appealing that the deficiencies in describing the intermolecular interactions with the standard force fields do not always lead to the fatal failure.<sup>86</sup> Therefore, in this work, eight sets of the standard force fields, OPT-FF,<sup>65</sup> AMBER 03,<sup>57</sup> GAFF,<sup>58</sup> OPLS-AA,<sup>43</sup> OPLS-CS,<sup>49</sup> CHARMM27,<sup>61,62</sup> GROMOS 53A5,<sup>63</sup> and GROMOS 53A6,<sup>63</sup> that were obtained under different specific backgrounds, are worth being further examined in the investigation for the nature of liquid benzene.

**3.2. Spatial Structures and Aromatic  $\pi$ – $\pi$  Interactions.** To obtain the overall features of the liquid structure with the different force fields, the radial distribution functions g(r) of both the center of mass (COM) and the carbon atoms of two benzene molecules are calculated and compared with the experimental results cited from refs 38 and 41. As shown in Figure 2, one can find that the deviations from the experimental data are distinctly large for the OPLS-CS and OPT-FF force fields,

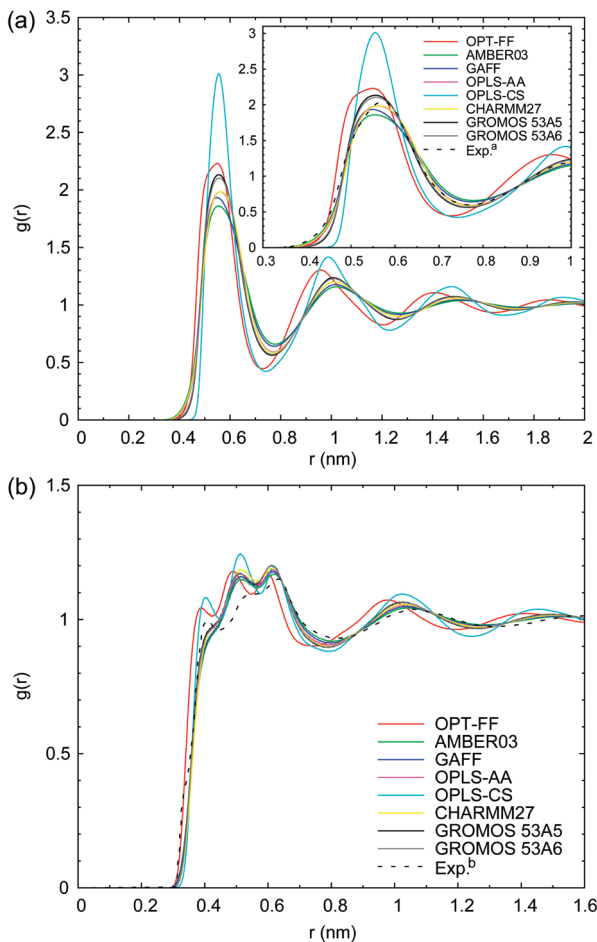


**Figure 2.** The radial distribution functions for the center of mass of benzene molecules (a) and the C–C atoms of benzene molecules (b). (a) Experimental data cited from ref 41. (b) Experimental data cited from ref 38.

although the OPLS-CS simulations were previously proved to be much better than the OPLS results.<sup>49</sup> In the inside panel of Figure 2a, one can find more details in comparison with the experimental data<sup>41</sup> for the first shell of liquid benzene. Around the first peak of  $g(r)_{\text{COM–COM}}$  (ca. 5.5 Å), two GROMOS force fields exhibit almost identical profiles of  $g(r)$ , while the AMBER 03 and GAFF force fields predict lower  $g(r)$  values. The results of OPLS-AA and CHARMM27 are much closer to the experimental data, and the similar good agreements for  $g(r)_{\text{C–C}}$  (see Figure 2b) can be extended to the long-range structures of liquid benzene. In Figure 2b, the OPLS-CS and OPT-FF force fields predict well the first small peak of  $g(r)_{\text{C–C}}$ , but their simulated  $g(r)_{\text{C–C}}$  values are obviously larger than the experimental data.<sup>38</sup> All of the simulated results overestimate the intensity of  $g(r)_{\text{C–C}}$  at the second and third peaks, but except for OPT-FF force field, the predictions for the positions of the second and third peaks are acceptable. In the long-range region, two diffuse peaks predicted with the OPT-FF and OPLS-CS force fields shift to smaller  $r(\text{C–C})$  values, while the other force fields provide quite satisfying results. In general, both OPLS-CS and OPT-FF failed in predicting the liquid structures, although the OPLS-CS force field was always recommended<sup>49</sup> and applied in simulations of benzene and benzene-like liquids,<sup>41</sup> and the OPT-FF force field can reproduce the benzene–benzene interaction

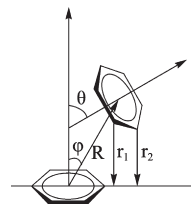


**Figure 3.** Diagram showing the definitions of  $\theta$ ,  $\varphi$ ,  $R$ ,  $r_1$ , and  $r_2$ .

potentials well.<sup>65</sup> Here, the other six sets of force fields, AMBER 03, GAFF, OPLS-AA, CHARMM27, GROMOS 53A5, and GROMOS 53A6, are proved to be reliable in the simulations of not only the local structures but also the long-range structures of liquid benzene.

To gain more features of the local structure, the populations of the different configurations of the benzene dimer in the first liquid shell are calculated. At first, five variables,  $\theta$ ,  $\varphi$ ,  $R$ ,  $r_1$ , and  $r_2$  as defined in Figure 3, are used as the criteria to identify the different configurations:  $R$  is the distance between the COMs of two benzene molecules;  $\theta$  is the angle between the two benzene planes;  $\varphi$  is the angle formed by the normal vector pointing from the COM of the bottom benzene to the COM of another benzene;  $r_1$  and  $r_2$  are the two smallest projection distances of two vicinal carbon atoms in the upper benzene onto the molecular plane of the bottom benzene. The criteria for the parallel, perpendicular, T, and Y configurations are given as follows: Parallel (including S and PD configurations),  $R \leq R_{\min}$ ,  $0^\circ \leq \theta \leq 40^\circ$ ; Perpendicular (including T and Y shapes),  $R \leq R_{\min}$ ,  $50^\circ \leq \theta \leq 90^\circ$ ,  $0^\circ \leq \varphi \leq 40^\circ$  or  $50^\circ \leq \varphi \leq 90^\circ$ , where  $R_{\min}$  is the  $r$  value for the first minimum of  $g(r)_{\text{COM–COM}}$  outside of the first shell (see Figure 2a), and it is varied with the different force fields. T-shape and Y-shape are further classified with  $|r_1 - r_2| \geq R_{CC}/4$  and  $|r_1 - r_2| < R_{CC}/4$ , respectively ( $R_{CC}$  is the carbon–carbon bond length of benzene). In Table 3, the differences of  $R_{\max}$  (the peak position) are less than 0.27 Å for the different force fields, while the differences of  $R_{\min}$  are less than 0.24 Å, with respect to the corresponding experimental values.<sup>41</sup> The  $R_{\max}$  value predicted with the CHARMM27 force field and the  $R_{\min}$  value predicted with the OPLS-CS force field are in the best agreement with the respective experimental values.<sup>41</sup> The coordination numbers predicted with all force fields are generally in accord with the experimental value of 12.<sup>41</sup> The OPLS-CS force field predicts the largest population of the perpendicular configurations (66.89%) and the smallest population for the parallel configurations (15.42%). Here, the parallel configuration is significantly disfavored, due to the separated charges of this force field. Since the larger interaction energies for the perpendicular (T and Y) configurations were calculated with high-level quantum chemistry methods,<sup>33,34</sup> the OPT-FF force field on the basis of the fittings to the *ab initio* results<sup>65</sup> certainly predicts the second largest population for the perpendicular configurations (59.59%) and the second smallest population for the parallel configurations (21.84%). The population sequence of the perpendicular configurations for the other force fields, GROMOS 53A5 ~ GROMOS 53A6 > OPLS-AA ~ GAFF > CHARMM27 > AMBER 03, is consistent with the interaction energy order calculated with these force fields (see Table 2). The population distributions of the parallel configurations are in a similar scenario. For the S and PD configurations, since the interaction energies predicted with two GROMOS force fields are much smaller than those with the AMBER 03, GAFF,

**Table 3. Location of the maxima ( $R_{\max}$ ) and the End of the First Peak ( $R_{\min}$ ) of the Radial Distribution Function  $g(r)_{\text{COM-COM}}$ , the Coordination Number for the First Shell, and the Populations of the Different Configurations of the Benzene Dimer in the First Liquid Shell**

	$R_{\max}$ (Å)	$R_{\min}$ (Å)	coordination number ( $r \sim 0.0 - R_{\min}$ Å)	parallel (%)	perpendicular (%)	T-shaped (%)	Y-shaped (%)
OPT-FF	5.48	7.26	12.8	21.84	59.59	25.98	33.60
AMBER 03	5.54	7.74	12.2	24.44	56.33	25.44	30.89
GAFF	5.50	7.74	12.4	24.04	56.83	25.80	31.03
OPLS-AA	5.62	7.68	12.4	23.72	57.07	25.77	31.30
OPLS-CS	5.54	7.38	12.5	15.42	66.89	27.90	38.99
CHARMM27	5.64	7.68	12.5	24.22	56.50	25.61	30.89
GROMOS 53A5	5.54	7.64	12.5	22.25	58.96	26.45	32.50
GROMOS 53A6	5.58	7.66	12.5	22.55	58.58	26.37	32.22
expt. <sup>41</sup>	5.75	7.50	~12				

OPLS-AA, and CHARMM27 force fields, the populations of the parallel configurations are relatively minor for the former force fields. It is interesting that all force fields predict isoenergetic interactions for the T- and Y-shaped dimers, but the populations of T and Y configurations in the liquid are distinctly different. For all of the force fields, the average ratio of the population, Y/T  $\approx$  1.25:1, is consistent with the experimental conclusion that the Y configuration is more favored than the T configuration in liquid benzene.<sup>41</sup> Generally, the population of the perpendicular configuration is 1 to 2 times more than that of the parallel configuration in the first shell. However, as pointed out by Headen et al.,<sup>41</sup> at a small molecular separation (<0.50 nm), the PD configurations are preferred, while at a larger separation (>0.50 nm), the neighboring aromatic rings are predominantly perpendicular to each other. The spatial scale of the first liquid shell discussed above ( $\leq 0.75$  nm) is just beyond the sensitive criterion of 0.50 nm given by Headen et al.<sup>41</sup> Therefore, to further analyze the different configuration populations dependent on the molecular separations in the first shell, we explore the molecular orientations and anisotropism in the first shell.

In Figure 4, the number of benzene molecules in the first shell is plotted as a function of the angle  $\theta$  between the two molecular planes. The molecular orientations of the first shell of benzene have been proved to be nearly isotropic in the experiment,<sup>41</sup> which is successfully reproduced in the present simulations with the AMBER 03, GAFF, OPLS-AA, CHARMM27, GROMOS 53A5, and GROMOS 53A6 force fields. In Figure 4, only the results of the OPT-FF (the upper panel in Figure 4a) and OPLS-CS (the upper panel in Figure 4e) force fields are distinctly different, indicating the large deviations from the isotropism at  $\theta \sim 90^\circ$ . When we turn back to the argument of whether the preferred parallel  $\pi-\pi$  contacts (PD) at the small molecular separation (<0.50 nm)<sup>41</sup> could be reproduced in the simulations, in the middle panels of Figure 4a–h, one can find that the AMBER 03, GAFF, OPLS-AA, and CHARMM27 force fields used in the simulations are approved to be reliable, supporting the experimental result;<sup>41</sup> the OPT-FF and OPLS-CS results are significantly different, violating Headen's conclusion;<sup>41</sup> the nearly isotropic distribution is found in the range of  $\theta$  from 0–20° for two GROMOS force fields, implying homogeneous configurations on this spatial scale. When the molecular separation is more than 0.50 nm (see the below panels), all of the simulations show that the perpendicular configuration is favored; in particular, the OPLS-CS model exhibits the largest deviation from the isotropic distribution. The molecular orientations in the

liquid must be closely related to the intermolecular interactions. In Figure 5, the contour maps of the benzene–benzene interaction energy can let readers more easily catch the major characteristics of the different force fields. In the calculations of these benzene–benzene interaction energy potentials, the benzene molecule at the bottom (see Figure 3) is fixed while the upper molecule rotates by changing  $\theta$  from 0 to 90°. Within the interaction energy range of –4.5 to 6.0 kcal/mol, two basins (two local existing minima that correspond to the parallel and perpendicular configurations) are clearly shown on the potential energy surfaces obtained with the OPT-FF, AMBER 03, OPLS-AA, and CHARMM27 force fields. At a small molecular separation ( $R < 0.50$  nm), only the perpendicular configurations (T and Y) are permitted for OPLS-CS. As for the OPT-FF force field, its potential well for the perpendicular configuration having a considerable large interaction energy (–2.5 kcal/mol) extends to the small molecular separation (<0.50 nm). This leads to the predominant perpendicular orientations in the small molecular separation region (<0.50 nm) at about 60°, corresponding to a maximum of the  $N(\theta)$  values in the middle panel of Figure 4a.

What is the physical factor playing a role in the preference of the parallel configuration at a small separation? According to the compositions of these force fields, see eq 1, the total potential energy at a separation distance of 0.45 nm (plotted in Figure 6a) is further decomposed to the Coulomb contribution (see Figure 6b), the intermolecular Lennard-Jones interactions between carbon and carbon atoms in two benzenes (see Figure 6c), the intermolecular Lennard-Jones interactions between carbon atoms in one benzene and hydrogen atoms in the other (see Figure 6d), and the intermolecular Lennard-Jones interactions between hydrogen and hydrogen atoms in two benzenes (see Figure 6e). As shown in Figure 6b, one can find that the strong Coulomb attractions lead to a preference of the perpendicular configuration for the OPLS-CS force field. For the OPT-FF force field, the remarkable large Lennard-Jones attraction in whole range of  $\theta$ , shown in Figure 6c, mainly arises from the largest  $\epsilon_C$  of this force field (see Table 1); in Figure 6d, the much weaker Lennard-Jones repulsive interaction around  $\theta \approx 90^\circ$  is due to the smallest values of  $\sigma_H$  and  $\epsilon_H$  (see Table 1). The intermolecular Lennard-Jones attractions (–1.2 to –1.7 kcal/mol, see Figure 6c) between carbon atoms should be responsible for the formation of the parallel configuration; moreover, as shown in Figure 6d, the perpendicular configuration is disfavored due to the relatively strong repulsive Lennard-Jones interactions between carbon atoms in one benzene and hydrogen atoms in another benzene. As shown in

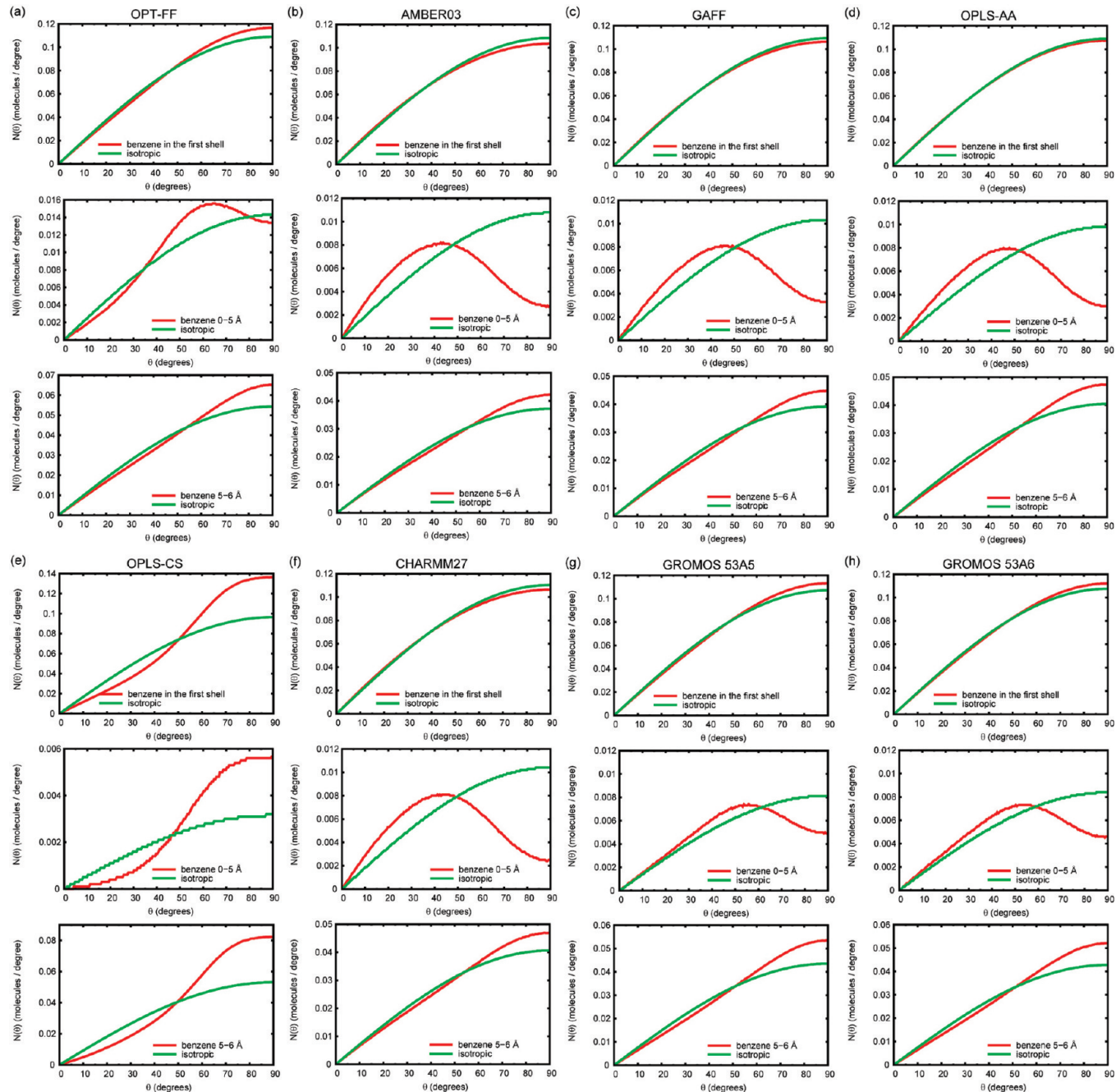


**Figure 4.** Number of benzene molecules in the first coordination shell as a function of the angle  $\theta$  between the aromatic planes (red lines). The green lines represent a random isotropic distribution of molecules.

Figure 6e, the intermolecular Lennard-Jones attractions between hydrogen atoms are too weak ( $<0.2$  kcal/mol) to influence the orientations of the benzene molecule.

**3.3. Thermodynamic Properties.** The accuracy of the structure calculated from MD simulations can discern the excellence of the different force fields. On the other hand, the thermodynamic properties predicted by MD simulations are also important in evaluating the superiority of the force fields. In Table 4, the density ( $\rho$ ), molecular volume ( $V$ ), heat capacity at constant pressure ( $C_p(l)$ ), vaporization enthalpy ( $\Delta H_{vap}$ ), shear viscosity ( $\eta$ ), self-diffusion coefficient ( $D$ ), and rotational correlation times of vectors perpendicular and parallel to the aromatic

plane ( $\tau_{2\perp}$  and  $\tau_{2||}$ ) for the different force fields used in the simulations are listed and compared with the experimental values cited from refs 72 and 87–90. The statistic errors of the theoretical values are also estimated with the methods proposed before.<sup>80</sup> The density,  $\rho = 870.4 \pm 0.6$  kg/m<sup>3</sup>, predicted with the CHARMM27 force field is in excellent agreement with the experimental result, while the AMBER 03 result is the smallest. The results of the OPLS-AA, GAFF, and two GROMOS force fields can also provide good results, within percent deviations of less than 3%. The percent deviations for the OPLS-CS and OPT-FF force fields reach 8.4% and 19.6%, respectively. The overestimated density of the OPT-FF force field may be attributed to

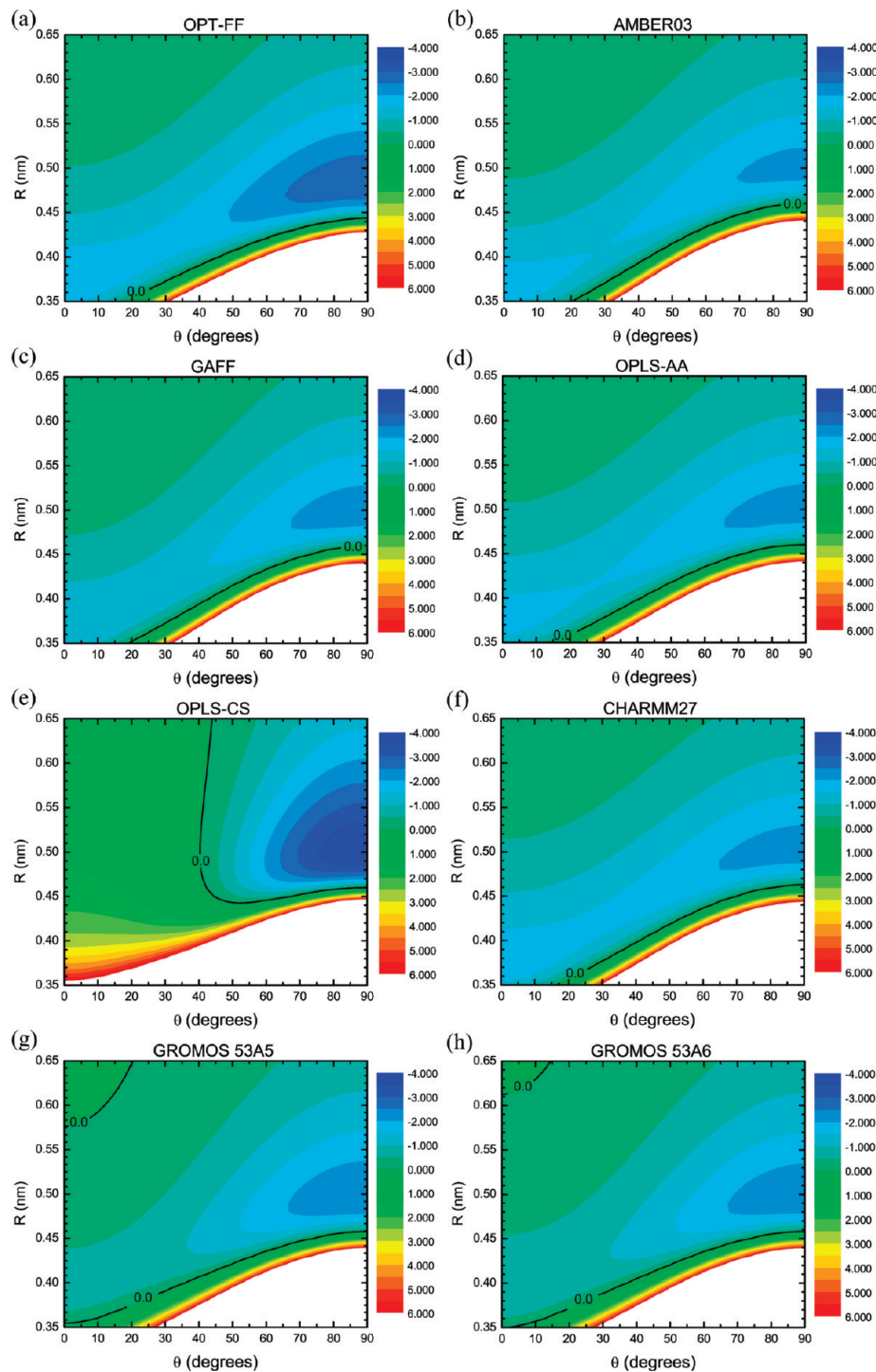


**Figure 5.** Contour maps ( $\theta \sim R_{\text{COM-COM}}$ ,  $\varphi = 0^\circ$ ) of the interaction potential energy surfaces of the benzene dimer. The black lines represent the contour line of 0 kcal/mol.

its quite small  $\sigma_H$  (see Table 1), which leads to a significant decrease of the molecular volume ( $V = 124.2 \pm 0.1 \text{ \AA}^3$ ).

The  $C_p(l)$  and  $\Delta H_{\text{vap}}$  values predicted with the OPLS-AA force field match the experimental data very well.<sup>72,87</sup> Within the computational uncertainty of  $C_p(l)$ , the result for the OPT-FF force field is also acceptable. The  $C_p(l)$  values of the CHARMM27 and two GROMOS force fields are a little larger than the experimental datum,<sup>87</sup> but the largest one,  $39.1 \pm 1.2 \text{ cal mol}^{-1}$

$\text{K}^{-1}$ , is predicted with the GAFF force field, and the smallest one,  $28.6 \pm 0.5 \text{ cal mol}^{-1} \text{ K}^{-1}$ , is estimated with the OPLS-CS force field. The two largest  $\Delta H_{\text{vap}}$  values are predicted with the OPT-FF and OPLS-CS force fields, while the results with the AMBER 03 and GAFF force fields are much smaller than the experimental datum.<sup>72</sup> However, the predictions of  $\Delta H_{\text{vap}}$  for most force fields except for the OPT-FF and OPLS-CS force fields are acceptable because of the large experimental uncertainty of

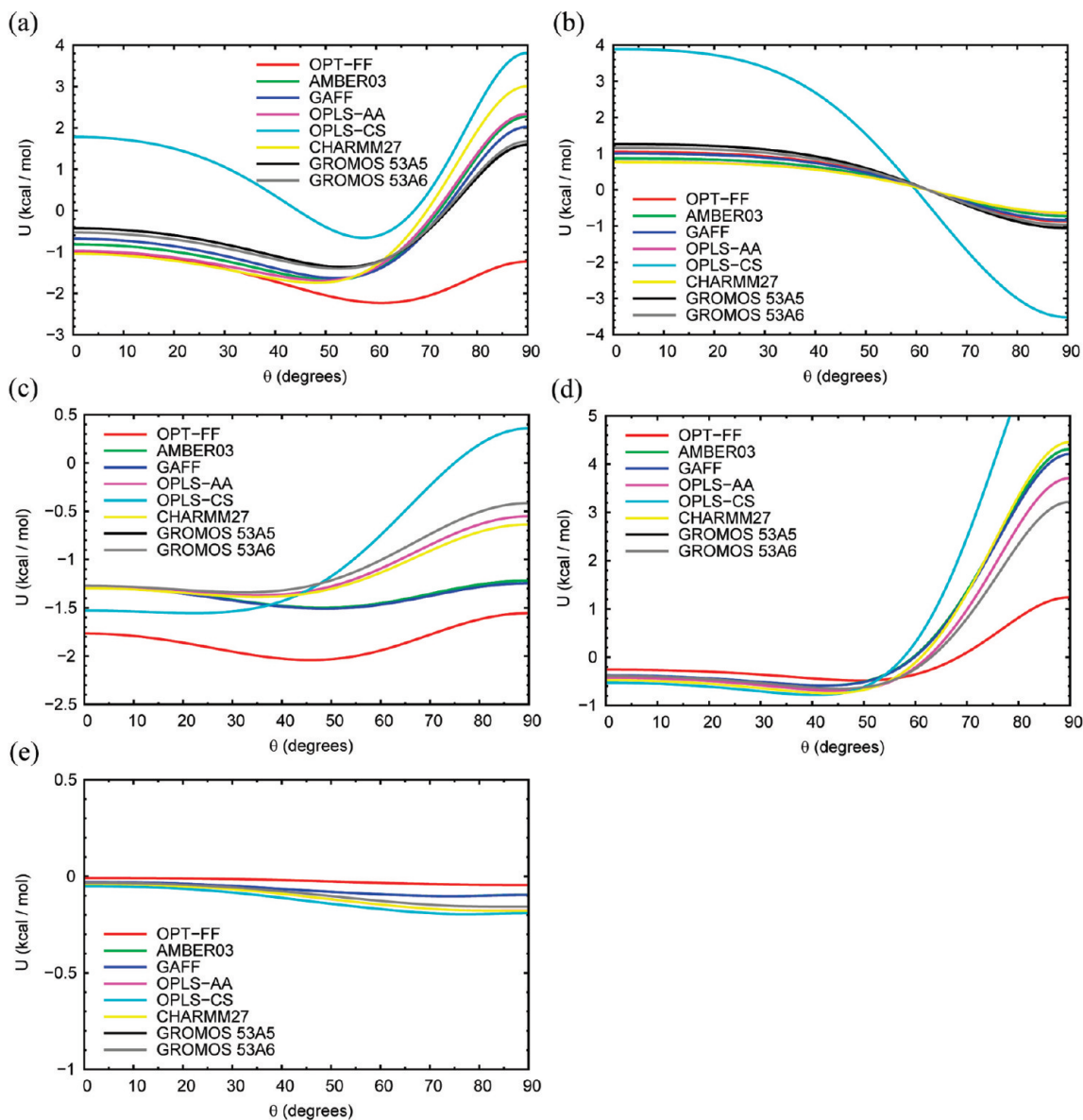


**Figure 6.** The potential energy curves of the benzene dimer as a function of the angle  $\theta$  between the aromatic planes ( $\varphi = 0^\circ$  and  $R_{\text{COM-COM}} = 0.45 \text{ nm}$ ). (a) The total intermolecular potential energy of the benzene dimer. (b) The Coulomb potential energy of the benzene dimer. (c) The intermolecular Lennard-Jones potential energy between carbon and carbon atoms in two benzene molecules. (d) The intermolecular Lennard-Jones potential energy between carbon atoms in one benzene and hydrogen atoms in the other benzene. (e) The intermolecular Lennard-Jones potential energy between hydrogen and hydrogen atoms in two benzene molecules.

$\Delta H_{\text{vap}}$  ( $\pm 0.48 \text{ kcal/mol}$ ).<sup>72</sup> In the scheme of the definitions of  $C_P(l)$  and  $\Delta H_{\text{vap}}$  (see eqs 2–4), we think that the distinct differences of these thermodynamic values are basically arising from the fluctuation discrepancies of intermolecular energies  $E_{\text{inter}}$  for these force fields. The significant differences of the intermolecular  $\pi-\pi$  interaction energies for these force fields have been discussed above. Moreover, the differences of  $V$  shown in Table 4 should be considered. The estimated  $C_P(l)$  and  $\Delta H_{\text{vap}}$  can also be influenced by the cutoffs of the long-range potential employed in the simulations.<sup>91,92</sup> The common values of the cutoff of 1.3 nm for the Coulomb interactions and the cutoff of 1.5 nm for van der Waals interactions were used in the present simulations for these different force fields. For example, in eq 1, the smaller atomic charges (e.g., those of OPLS-AA and CHARMM27, see Table 1) can lead to the quick quenching of the Coulomb interaction, while

the larger charges used in the Coulomb potential calculations may need the larger cutoff value.

The viscosity, as a kinetic property, is not only important for pure liquids, as it also influences the rates of diffusion and conformational change of molecules solvated in the liquid. Thus, it is important that the force field can predict the accurate value of viscosity of liquids. The shear viscosity of liquid benzene for the different force fields calculated from the nonequilibrium MD simulations is compared with the experimental result<sup>88</sup> in Table 4. The CHARMM27 force field predicts the best value, with respect to the experimental datum.<sup>88</sup> The results of the OPLS-AA and GROMOS 53A6 force fields are also outstanding, and they have percent deviations of 9.0% and 9.8%, respectively. Unfortunately, quite large values with percent deviations of 39.4%, 28.3%, and 21.3% are predicted with the AMBER 03, GAFF, and GROMOS

**Table 4.** Some Thermodynamic Properties Calculated from the MD Simulations Using the Different Force Fields

	$\rho$ (kg/m <sup>3</sup> )	$V$ (Å <sup>3</sup> )	$C_p(l)$ (cal mol <sup>-1</sup> K <sup>-1</sup> )	$\Delta H_{vap}$ (kcal/mol)	$\eta$ (10 <sup>-3</sup> kg m <sup>-1</sup> s <sup>-1</sup> )	$D$ (10 <sup>-9</sup> m <sup>2</sup> /s)	$\tau_{2\perp}$ (ps)	$\tau_{2  }$ (ps)
OPT-FF	1044.6 ± 0.6	124.2 ± 0.1	35.2 ± 1.3	11.30 ± 0.02	3.280 ± 0.031	0.35 ± 0.01	6.16	2.53
AMBER 03	835.9 ± 0.5	155.2 ± 0.1	36.6 ± 1.3	7.24 ± 0.01	0.364 ± 0.003	2.79 ± 0.22	1.40	1.09
GAFF	852.1 ± 0.8	152.2 ± 0.2	39.1 ± 1.2	7.55 ± 0.01	0.431 ± 0.002	2.33 ± 0.01	1.71	1.24
OPLS-AA	867.3 ± 0.4	149.6 ± 0.1	33.3 ± 0.8	8.02 ± 0.01	0.547 ± 0.004	1.97 ± 0.10	1.59	1.19
OPLS-CS	947.2 ± 0.3	136.9 ± 0.1	28.6 ± 0.5	14.86 ± 0.01	<sup>a</sup>	<sup>a</sup>	<sup>a</sup>	<sup>a</sup>
CHARMM27	870.4 ± 0.6	149.0 ± 0.2	37.6 ± 1.2	8.17 ± 0.01	0.567 ± 0.003	1.97 ± 0.17	1.41	1.10
GROMOS 53A5	887.3 ± 0.2	146.2 ± 0.1	37.3 ± 0.7	8.44 ± 0.01	0.729 ± 0.004	1.53 ± 0.02	2.07	1.30
GROMOS 53A6	881.5 ± 0.3	147.2 ± 0.1	37.2 ± 0.6	8.25 ± 0.01	0.660 ± 0.005	1.78 ± 0.04	1.79	1.19
exptl.	873.8 <sup>b</sup>	148.4 <sup>b</sup>	32.4 <sup>c</sup>	7.89 ± 0.48 <sup>b</sup>	0.601 <sup>d</sup>	2.20 <sup>e</sup>	1.68 <sup>f</sup>	1.29 <sup>f</sup>

<sup>a</sup>The unreliable values of  $\eta$ ,  $D$ ,  $\tau_{2\perp}$ , and  $\tau_{2||}$  are predicted with OPLS-CS force field. <sup>b</sup>Cited from ref 72. <sup>c</sup>Cited from ref 87. <sup>d</sup>Cited from ref 88. <sup>e</sup>Cited from ref 89. <sup>f</sup>Cited from ref 90.

S3A5 force fields, respectively. The result of the OPT-FF force field is nearly 5 times higher than the experimental datum.<sup>88</sup> What is more, the viscosity cannot be derived with the OPLS-CS force field. In the nonequilibrium simulations, see eq 14, the different densities  $\rho$  used for the various force fields may numerically influence the shear viscosity. However, for certain density values with the same percent deviation derived with different force fields, their corresponding shear viscosities can be significantly different, thus such a numerical effect of  $\rho$  should be neglected. The differences in the fluidity of liquid benzene determined by these force fields should mainly come from the deviations of the descriptions of the intermolecular  $\pi-\pi$  interactions. The rather large density and interaction energies of the different configurations of the benzene dimer for the OPT-FF force field may significantly impair the fluidity of liquid benzene, namely, result in a larger shear viscosity. The separated charges used in the OPLS-CS force field overemphasize the perpendicular orientations of benzene molecules; thus the fluidity of liquid benzene may be hindered by the strong attractive interaction energies of the perpendicular configurations.

The self-diffusion coefficient  $D$  predicted from the MD simulations is another important property to account for the force fields. The GAFF force field can predict quite well the experimental value<sup>89</sup> with a percent deviation of 5.9%. The OPLS-AA and CHARMM27 force fields also gain reasonable values with percent deviations of 10.5%. Furthermore, within the statistical uncertainties for the OPLS-AA and CHARMM27 force fields, their theoretical values may be more acceptable. Unfortunately, the results of the AMBER 03, GROMOS 53A5, and GROMOS 53A6 force fields have large deviations from the experimental value<sup>89</sup> with percent deviations of 26.8%, 30.5%, and 19.1%, respectively. The result of the OPT-FF force field is almost 1 order of magnitude smaller than the experimental value.<sup>89</sup> What is more, the OPLS-CS force field fails again in the prediction of the self-diffusion coefficient of liquid benzene.

The rotational correlation times of the vectors perpendicular and parallel to the aromatic plane ( $\tau_{2\perp}$  and  $\tau_{2||}$ ) are evaluated with the different force fields. For all of these force fields,  $\tau_{2\perp} > \tau_{2||}$ , which is consistent with the experimental datum.<sup>90</sup> The GAFF force field obtains perfect values of both  $\tau_{2\perp}$  and  $\tau_{2||}$  with percent deviations of 1.8% and 3.9%, respectively. Although GROMOS 53A5 predicts the best values of  $\tau_{2||}$  (only with percent deviation of 0.8%), the value of  $\tau_{2\perp}$  evaluated by this force field is much larger than the experimental datum<sup>90</sup> (with a percent deviation of 23.2%). The results of both  $\tau_{2\perp}$  and  $\tau_{2||}$  predicted with the OPLS-AA and GROMOS 53A6 force fields are acceptable, with percent deviations of 5.4% and 6.5% for  $\tau_{2\perp}$ , respectively, and both being 7.8% for  $\tau_{2||}$ . However, the results

predicted with the OPT-FF, AMBER 03, and CHARMM27 force fields show quite large percent deviations, namely, 266.7%, 16.7%, and 16.1% for  $\tau_{2\perp}$  and 96.1%, 15.5%, and 14.7% for  $\tau_{2||}$ , respectively. Unfortunately, the OPLS-CS force field fails again in predicting either  $\tau_{2\perp}$  or  $\tau_{2||}$ .

As mentioned above, the dynamic properties  $D$  and  $\tau_2$  show significant differences for these sets of force fields, which should be closely related to the distinct differences in description of the intermolecular interactions. For instance, the relatively strong attractive interactions in the perpendicular configuration of the benzene dimer that are predicted with the OPT-FF and OPLS-CS force fields assuredly lead to much smaller self-diffusion coefficients (nearly zero for OPLS-CS); moreover, the relaxation time  $\tau_{2\perp}$  is seriously overestimated or irregularly larger than  $\tau_{2||}$ , e.g., for OPLS-CS,  $\tau_{2\perp} \sim 3.02 \times 10^{33}$  ps while  $\tau_{2||} \sim 2.14 \times 10^3$  ps. The overestimation of the  $\pi-\pi$  attractive interactions and the overemphasis on a certain configuration (e.g., the perpendicular configuration for OPLS-CS) will remarkably influence the simulation results of the structural and dynamic properties of liquid benzene.

#### 4. CONCLUSION

In the present study, the classical MD simulations of liquid benzene are performed with the recently developed force fields OPT-FF,<sup>65</sup> AMBER 03,<sup>57</sup> GAFF,<sup>58</sup> OPLS-AA,<sup>43</sup> OPLS-CS,<sup>49</sup> CHARMM27,<sup>61,62</sup> GROMOS 53A5,<sup>63</sup> and GROMOS 53A6.<sup>63</sup> To evaluate the qualities of these force fields, our strategy was as follows: First, the potential energy curves of the benzene dimer at four different configurations, S, PD, T, and Y-shaped, were predicted with these force fields and compared with the high-level quantum chemistry results.<sup>33,34</sup> Second, with the references of the experimental studies,<sup>38,41</sup> the local and long-range structures of liquid benzene were carefully examined on the basis of the present simulations. Third, the thermodynamic properties were calculated and compared with the experimental datum.<sup>72,87–90</sup> In the last two parts, the significant differences of the simulations using the various force fields were discussed in detail, in which we particularly pursued the physical diversities in the description of aromatic  $\pi-\pi$  interactions for these force fields. Conclusive remarks are summarized here:

- (1) On the local structures of liquid benzene, the parallel PD configuration at a small separation is favored.<sup>41</sup> As shown in Figure 6, this can be reasonably interpreted with the intermolecular Lennard-Jones attractions between carbon and carbon atoms in two benzene molecules in the parallel configuration, while the intermolecular Lennard-Jones

interactions between carbon and hydrogen atoms in the perpendicular configuration are strongly repulsive.

- (2) The AMBER 03, GAFF, OPLS-AA, and CHARMM27 force fields are reliable in the description of the orientational distribution of benzene molecules in the first coordination shell. However, the preference for the parallel configurations at a small molecular separation ( $<0.50$  nm) cannot be reproduced in the simulations with the OPT-FF, GROMOS 53AS, and GROMOS 53A6 force fields, which is due to the largest  $\epsilon_C$  and the smallest  $\sigma_H$  and  $\epsilon_H$  used in OPT-FF and the relatively large point charges on the C and H atoms used in the two GROMOS force fields. The separated charges used in the OPLS-CS force field result in the perpendicular configuration being strongly preferred. Through careful examinations of the simulated results using these different force fields, we recommend that the OPLS-AA force field is the best one, not only in the descriptions of the microstructures of liquid benzene but also in the thermodynamic properties investigated in this work. The OPLS-AA force field is promising for the applications to the other aromatic  $\pi-\pi$  interaction systems.
  
- (3) For the aromatic  $\pi-\pi$  interaction systems, neither the exaggeration of the quadrupole–quadrupole interaction in the force field function (e.g., OPLS-CS<sup>49</sup>) nor merely fitting the *ab initio* pairwise interaction potentials (e.g., OPT-FF<sup>65</sup>) can simply warrant the reliability of these force fields. Thus, a highly qualified force field should be good at the descriptions on not only the microstructure but also at the predictions of the thermodynamic properties of the liquids.

## AUTHOR INFORMATION

### Corresponding Author

\*E-mail: [sxtian@ustc.edu.cn](mailto:sxtian@ustc.edu.cn).

## ACKNOWLEDGMENT

This work is partially supported by MOST (Grant Nos. 2007CB815204 and 2011CB921401).

## REFERENCES

- (1) Hunter, C. A. Aromatic Interactions in Proteins, DNA and Synthetic Receptors. *Philos. Trans. R. Soc. London, Ser. A* **1993**, *345*, 77.
- (2) Burley, S. K.; Petsko, G. A. Aromatic-Aromatic Interaction: A Mechanism of Protein Structure. *Science* **1985**, *229*, 23.
- (3) Hunter, C. A.; Singh, J.; Thornton, J. M.  $\pi-\pi$  Interactions: The Geometry and Energetics of Phenylalanine-Phenylalanine Interaction in Proteins. *J. Mol. Biol.* **1991**, *218*, 837.
- (4) Ranganathan, D.; Haridas, V.; Gilardi, R.; Karle, I. L. Self-Assembling Aromatic-Bridged Serine-Based Cyclodepsipeptides (Serinophanes): A Demonstration of Tubular Structures Formed through Aromatic  $\pi-\pi$  Interactions. *J. Am. Chem. Soc.* **1998**, *120*, 10793.
- (5) Vondrášek, J.; Bendová, L.; Klusák, V.; Hobza, P. Unexpectedly Strong Energy Stabilization Inside the Hydrophobic Core of Small Protein Rubredoxin Mediated by Aromatic Residues: Correlated Ab Initio Quantum Chemical Calculations. *J. Am. Chem. Soc.* **2005**, *127*, 2615.
- (6) Frederick, C. A.; Williams, L. D.; Ughetto, G.; van der Marel, G. A.; van Boom, J. H.; Rich, A.; Wang, A. H.-J. Structural Comparison of Anticancer Drug-DNA Complexes: Adriamycin and Daunomycin. *Biochemistry* **1990**, *29*, 2538.
- (7) Meyer, E. A.; Castellano, R. K.; Diederich, F. Interactions with Aromatic Rings in Chemical and Biological Recognition. *Angew. Chem., Int. Ed.* **2003**, *42*, 1210.
- (8) Evans, D. A.; Chapman, K. T.; Hung, D. T.; Kawaguchi, A. T. Transition State  $\pi$ -Solvation by Aromatic Rings: An Electronic Contribution to Diels-Alder Reaction Diastereoselectivity. *Angew. Chem., Int. Ed. Engl.* **1987**, *26*, 1184.
- (9) Quiocho, F. A.; Vyas, N. K. Novel Stereospecificity of the L-arabinose-Binding Protein. *Nature* **1984**, *310*, 381.
- (10) Vyas, N. K.; Vyas, M. N.; Quiocho, F. A. A Novel Calcium Binding Site in the Galactose-Binding Protein of Bacterial Transport and Chemotaxis. *Nature* **1987**, *327*, 635.
- (11) Benzing, T.; Tjivikua, T.; Wolfe, J.; Rebek, J., Jr. Recognition and Transport of Adenine Derivatives with Synthetic receptors. *Science* **1988**, *242*, 266.
- (12) Vyas, N. K.; Vyas, M. N.; Quiocho, F. A. Sugar and Signal-Transducer Binding Sites of the Escherichia Coli Galactose Chemoreceptor Protein. *Science* **1988**, *242*, 1290.
- (13) Muehldorf, A. V.; van Engen, D.; Warner, J. C.; Hamilton, A. D. Aromatic-Aromatic Interactions in Molecular Recognition: A Family of Artificial Receptors for Thymine That Shows Both Face-to-Face and Edge-to-Face Orientations. *J. Am. Chem. Soc.* **1988**, *110*, 6561.
- (14) Desiraju, G. R.; Gavezzotti, A. From Molecular to Crystal Structure; Polynuclear Aromatic Hydrocarbons. *J. Chem. Soc., Chem. Commun.* **1989**, *621*.
- (15) Ferguson, S. B.; Sanford, E. M.; Seward, E. M.; Diederich, F. Cyclophane-Arene Inclusion Complexation in Protic Solvents: Solvent Effects versus Electron Donor-Acceptor Interactions. *J. Am. Chem. Soc.* **1991**, *113*, 5410.
- (16) Vallée, R.; Damman, P.; Dosière, M.; Toussaint, E.; Zyss, J. Nonlinear Optical Properties and Crystalline Orientation of 2-Methyl-4-nitroaniline Layers Grown on Nanostructured Poly(tetrafluoroethylene) Substrates. *J. Am. Chem. Soc.* **2000**, *122*, 6701.
- (17) Janda, K. C.; Hemminger, J. C.; Winn, J. S.; Novick, S. E.; Harris, S. J.; Klemperer, W. Benzene Dimer: A Polar Molecule. *J. Chem. Phys.* **1975**, *63*, 1419.
- (18) Steed, J. M.; Dixon, T. A.; Klemperer, W. Molecular Beam Studies of Benzene Dimer, Hexafluorobenzene Dimer, and Benzene-Hexafluorobenzene. *J. Chem. Phys.* **1979**, *70*, 4940.
- (19) Hopkins, J. B.; Powers, D. E.; Smalley, R. E. Mass-Selective Two-Color Photoionization of Benzene Clusters. *J. Phys. Chem.* **1981**, *85*, 3739.
- (20) Langridge-Smith, P. R. R.; Brumbaugh, D. V.; Haynam, C. A.; Levy, D. H. Ultraviolet Spectra of Benzene Clusters. *J. Phys. Chem.* **1981**, *85*, 3742.
- (21) Krause, H.; Ernstberger, B.; Neusser, H. J. Binding Energies of Small Benzene Clusters. *Chem. Phys. Lett.* **1991**, *184*, 411.
- (22) Henson, B. F.; Hartland, G. V.; Venturo, V. A.; Felker, P. M. Raman-Vibronic Double-Resonance Spectroscopy of Benzene Dimer Isotopomers. *J. Chem. Phys.* **1992**, *97*, 2189.
- (23) Venturo, V. A.; Felker, P. M. Intermolecular Raman Bands in the Ground State of Benzene Dimer. *J. Chem. Phys.* **1993**, *99*, 748.
- (24) Erlekam, U.; Frankowski, M.; Meijer, G.; von Helden, G. An Experimental Value for the  $B_{1u}$  C-H Stretch Mode in Benzene. *J. Chem. Phys.* **2006**, *124*, 171101.
- (25) Erlekam, U.; Frankowski, M.; von Helden, G.; Meijer, G. Cold Collisions Catalyze Conformational Conversion. *Phys. Chem. Chem. Phys.* **2007**, *9*, 3786.
- (26) Hobza, P.; Selzle, H. L.; Schlag, E. W. Floppy Structure of the Benzene Dimer: Ab Initio Calculation on the Structure and Dipole Moment. *J. Chem. Phys.* **1990**, *93*, 5893.
- (27) Hobza, P.; Selzle, H. L.; Schlag, E. W. Potential Energy Surface for the Benzene Dimer. Results of Ab Initio CCSD(T) Calculations Show Two Nearly Isoenergetic Structures: T-Shaped and Parallel-Displaced. *J. Phys. Chem.* **1996**, *100*, 18790.
- (28) Sinnokrot, M. O.; Valeev, E. F.; Sherill, C. D. Estimates of the Ab Initio Limit for  $\pi-\pi$  Interactions: The Benzene Dimer. *J. Am. Chem. Soc.* **2002**, *124*, 10887.

- (29) Sinnokrot, M. O.; Sherill, C. D. Highly Accurate Coupled Cluster Potential Energy Curves for the Benzene Dimer: Sandwich, T-Shaped, and Parallel-Displaced Configurations. *J. Phys. Chem. A* **2004**, *108*, 10200.
- (30) Hesselmann, A.; Jansen, G.; Schütz, M. Density-Functional Theory-Symmetry-Adapted Intermolecular Perturbation Theory with Density Fitting: A New Efficient Method to Study Intermolecular Interaction Energies. *J. Chem. Phys.* **2005**, *122*, 014103.
- (31) Podeszwa, R.; Bukowski, R.; Szalewicz, K. Potential Energy Surface for the Benzene Dimer and Perturbational Analysis of  $\pi$ - $\pi$  Interactions. *J. Phys. Chem. A* **2006**, *110*, 10345.
- (32) Sinnokrot, M. O.; Sherill, C. D. High-Accuracy Quantum Mechanical Studies of  $\pi$ - $\pi$  Interactions in Benzene Dimers. *J. Phys. Chem. A* **2006**, *110*, 10656.
- (33) Sherrill, C. D.; Takatani, T.; Hohenstein, G. An Assessment of Theoretical Methods for Nonbonded Interactions: Comparison to Complete Basis Set Limit Coupled-Cluster Potential Energy Curves for the Benzene Dimer, the Methane Dimer, Benzene-Methane, and Benzene-H<sub>2</sub>S. *J. Phys. Chem. A* **2009**, *113*, 10146.
- (34) van der Avoird, A.; Podeszwa, R.; Szalewicz, K.; Leforestier, C.; van Harreveld, R.; Bunker, P. R.; Schnell, M.; von Helden, G.; Meijer, G. Vibration-Rotation-Tunneling States of the Benzene Dimer: An Ab Initio Study. *Phys. Chem. Chem. Phys.* **2010**, *12*, 8219.
- (35) Engkvist, O.; Hobza, P.; Selzle, H. L.; Schlag, E. W. Benzene Trimer and Benzene Tetramer: Structures and Properties Determined by the Nonempirical Model (NEMO) Potential Calibrated from the CCSD(T) Benzene Dimer Energies. *J. Chem. Phys.* **1999**, *110*, 5758.
- (36) Tauer, T. P.; Sherrill, C. D. Beyond the Benzene Dimer: An Investigation of the Additivity of  $\pi$ - $\pi$  Interactions. *J. Phys. Chem. A* **2005**, *109*, 10475.
- (37) Mahadevi, A. S.; Rahalkar, A. P.; Gadre, S. R.; Sastry, G. N. Ab Initio Investigation of Benzene Clusters: Molecular Tailoring Approach. *J. Chem. Phys.* **2010**, *133*, 164308.
- (38) Narten, A. H. X-Ray Diffraction Pattern and Models of Liquid Benzene. *J. Chem. Phys.* **1977**, *67*, 2102.
- (39) Misawa, M.; Fukunaga, T. Structure of Liquid Benzene and Naphthalene Studied by Pulsed Neutron Total Scattering. *J. Chem. Phys.* **1990**, *93*, 3495.
- (40) Cabaço, M. I.; Danten, Y.; Besnard, M.; Guissani, Y.; Guillot, B. Neutron Diffraction and Molecular Dynamics Study of Liquid Benzene and Its Fluorinated Derivatives as a Function of Temperature. *J. Phys. Chem. B* **1997**, *101*, 6977.
- (41) Headen, T. F.; Howard, C. A.; Skipper, N. T.; Wilkinson, M. A.; Bowron, D. T.; Soper, A. K. Structure of  $\pi$ - $\pi$  Interactions in Aromatic Liquids. *J. Am. Chem. Soc.* **2010**, *132*, 5735.
- (42) Evans, D. J.; Watts, R. O. On the Structure of Liquid Benzene. *Mol. Phys.* **1976**, *32*, 93.
- (43) OPLS: Jorgensen, W. L.; Tirado-Rives, J. The OPLS Potential Functions for Proteins. Energy Minimizations for Crystals of Cyclic Peptides and Crambin. *J. Am. Chem. Soc.* **1988**, *110*, 1657. OPLS-AA: Jorgensen, W. L.; Severance, D. L. Aromatic-Aromatic Interactions: Free Energy Profiles for the Benzene Dimer in Water, Chloroform, and Liquid Benzene. *J. Am. Chem. Soc.* **1990**, *112*, 4768.
- (44) Jorgensen, W. L.; Laird, E. R.; Nguyen, T. B.; Tirado-Rives, J. Monte Carlo Simulations of Pure Liquid Substituted Benzenes with OPLS Potential Functions. *J. Comput. Chem.* **1993**, *14*, 206.
- (45) Errington, J. R.; Panagiotopoulos, A. Z. New Intermolecular Potential Models for Benzene and Cyclohexane. *J. Chem. Phys.* **1999**, *111*, 9731.
- (46) Cacelli, I.; Cinacchi, G.; Prampolini, G.; Tani, A. Modeling >Benzene with Single-Site Potentials from Ab Initio Calculations: A Step toward Hybrid Models of Complex Molecules. *J. Chem. Phys.* **2004**, *120*, 3648.
- (47) Cacelli, I.; Cinacchi, G.; Prampolini, G.; Tani, A. Computer Simulation of Solid and Liquid Benzene with an Atomistic Interaction Potential Derived from Ab Initio Calculations. *J. Am. Chem. Soc.* **2004**, *126*, 14278.
- (48) Contreras-Camacho, R. O.; Ungerer, P.; Boutin, A.; Mackie, A. D. Optimized Intermolecular Potential for Aromatic Hydrocarbons Based on Anisotropic United Atoms. 1. Benzene. *J. Phys. Chem. B* **2004**, *108*, 14109.
- (49) Baker, C. M.; Grant, G. H. The Structure of Liquid Benzene. *J. Chem. Theory Comput.* **2006**, *2*, 947.
- (50) Bonnaud, P.; Nieto-Draghi, C.; Ungerer, P. Anisotropic United Atom Model Including the Electrostatic Interactions of Benzene. *J. Phys. Chem. B* **2007**, *111*, 3730.
- (51) Milet, A.; Korona, T.; Moszynski, R.; Kochanski, E. Anisotropic Intermolecular Interactions in van der Waals and Hydrogen-Bonded Complexes: What can We Get from Density Functional Calculations? *J. Chem. Phys.* **1999**, *111*, 7727.
- (52) Cybulski, S. M.; Seversen, C. E. Critical Examination of the Supermolecule Density Functional Theory Calculations of Intermolecular Interactions. *J. Chem. Phys.* **2005**, *122*, 014117.
- (53) Zhao, Y.; Truhlar, D. G. How Well Can New-Generation Density Functional Methods Describe Stacking Interactions in Biological Systems? *Phys. Chem. Chem. Phys.* **2005**, *7*, 2701.
- (54) Sato, T.; Tsuneda, T.; Hirao, K. A Density-Functional Study on  $\pi$ -Aromatic Interaction: Benzene Dimer and Naphthalene Dimer. *J. Chem. Phys.* **2005**, *123*, 104307.
- (55) Waller, M. P.; Robertazzi, A.; Platts, J. A.; Hibbs, D. E.; Williams, P. A. Hybrid Density Functional Theory for  $\pi$ -Stacking Interactions: Application to Benzenes, Pyridines, and DNA Bases. *J. Comput. Chem.* **2006**, *27*, 491.
- (56) Zhao, Y.; Schultz, N. E.; Truhlar, D. G. Design of Density Functionals by Combining the Method of Constraint Satisfaction with Parametrization for Thermochemistry, Thermochemical Kinetics, and Noncovalent Interactions. *J. Chem. Theory Comput.* **2006**, *2*, 364.
- (57) Duan, Y.; Wu, C.; Chowdhury, S.; Lee, M. C.; Xiong, G.; Zhang, W.; Yang, R.; Cieplak, P.; Luo, R.; Lee, T.; Caldwell, J.; Wang, J.; Kollman, P. A Point-Charge Force Field for Molecular Mechanics Simulations of Proteins Based on Condensed-Phase Quantum Mechanical Calculations. *J. Comput. Chem.* **2003**, *24*, 1999.
- (58) Wang, J.; Wolf, R. M.; Caldwell, J. W.; Kollman, P. A.; Case, D. A. Development and Testing of a General Amber Force Field. *J. Comput. Chem.* **2004**, *25*, 1157.
- (59) Jorgensen, W. L.; Maxwell, D. S.; Tirado-Rives, J. Development and Testing of the OPLS All-Atom Force Field on Conformational Energetics and Properties of Organic Liquids. *J. Am. Chem. Soc.* **1996**, *118*, 11225.
- (60) Kaminski, G. A.; Friesner, R. A.; Tirado-Rives, J.; Jorgensen, W. L. Evaluation and Reparametrization of the OPLS-AA Force Field for Proteins via Comparison with Accurate Quantum Chemical Calculations on Peptides. *J. Phys. Chem. B* **2001**, *105*, 6474.
- (61) MacKerell, A. D., Jr.; Bashford, D.; Bellott, M.; Dunbrack, R. L., Jr.; Evanseck, J. D.; Field, M. J.; Fischer, S.; Gao, J.; Guo, H.; Ha, S.; Joseph-McCarthy, D.; Kuchnir, L.; Kuczera, K.; Lau, F. T. K.; Mattos, C.; Michnick, S.; Ngo, T.; Nguyen, D. T.; Prodhom, B.; Reiher, W. E., III; Roux, B.; Schlenkrich, M.; Smith, J. C.; Stote, R.; Straub, J.; Watanabe, M.; Wiórkiewicz-Kuczera, J.; Yin, D.; Karplus, M. All-Atom Empirical Potential for Molecular Modeling and Dynamics Studies of Proteins. *J. Phys. Chem. B* **1998**, *102*, 3586.
- (62) MacKerell, A. D., Jr.; Feig, M.; Brooks, C. L., III. Extending the Treatment of Backbone Energetics in Protein Force Fields: Limitations of Gas-Phase Quantum Mechanics in Reproducing Protein Conformational Distributions in Molecular Dynamics Simulations. *J. Comput. Chem.* **2004**, *25*, 1400.
- (63) Oostenbrink, C.; Villa, A.; Mark, A. E.; van Gunsteren, F. A Biomolecular Force Field Based on the Free Enthalpy of Hydration and Solvation: The GROMOS Force-Field Parameter Sets 53A5 and 53A6. *J. Comput. Chem.* **2004**, *25*, 1656.
- (64) Hunter, A. C.; Sanders, J. K. The Nature of  $\pi$ - $\pi$  Interactions. *J. Am. Chem. Soc.* **1990**, *112*, 5525.
- (65) Sherrill, C. D.; Sumpter, B. G.; Sinnokrot, M. O.; Marshall, M. S.; Hohenstein, E. G.; Walker, R. C.; Gould, I. R. Assessment of Standard Force Field Models Against High-Quality Ab Initio Potential Curves for Prototypes of  $\pi$ - $\pi$ , CH/ $\pi$ , and SH/ $\pi$  Interactions. *J. Comput. Chem.* **2009**, *30*, 2187.

- (66) Bjelkmar, P.; Larsson, P.; Cuendet, M. A.; Bess, B.; Lindahl, E. Implementation of the CHARMM Force Field in GROMACS: Analysis of Protein Stability Effects from Correction Maps, Virtual Interaction Sites, and Water Models. *J. Chem. Theory Comput.* **2010**, *6*, 459.
- (67) Wang, J.; Wang, W.; Kollman, P. A.; Case, D. A. Automatic Atom Type and Bond Type Perception in Molecular Mechanical Calculations. *J. Mol. Graphics Modell.* **2006**, *25*, 247.
- (68) Bayly, C. I.; Cieplak, P.; Cornell, W. D.; Kollman, P. A. A Well-Behaved Electrostatic Potential Based Method Using Charge Restraints for Deriving Atomic Charges: The RESP Model. *J. Phys. Chem.* **1993**, *97*, 10269.
- (69) Frisch, M. J.; Trucks, G. W.; Schlegel, H. B.; Scuseria, G. E.; Robb, M. A.; Cheeseman, J. R.; Montgomery, J. A., Jr.; Vreven, T.; Kudin, K. N.; Burant, J. C.; Millam, J. M.; Iyengar, S. S.; Tomasi, J.; Barone, V.; Mennucci, B.; Cossi, M.; Scalmani, G.; Rega, N.; Petersson, G. A.; Nakatsuji, H.; Hada, M.; Ehara, M.; Toyota, K.; Fukuda, R.; Hasegawa, J.; Ishida, M.; Nakajima, T.; Honda, Y.; Kitao, O.; Nakai, H.; Klene, M.; Li, X.; Knox, J. E.; Hratchian, H. P.; Cross, J. B.; Adamo, C.; Jaramillo, J.; Gomperts, R.; Stratmann, R. E.; Yazyev, O.; Austin, A. J.; Cammi, R.; Pomelli, C.; Ochterski, J. W.; Ayala, P. Y.; Morokuma, K.; Voth, G. A.; Salvador, P.; Dannenberg, J. J.; Zakrzewski, V.; Dapprich, G.; S.; Daniels, A. D.; Strain, M. C.; Farkas, O.; Malick, D. K.; Rabuck, A. D.; Raghavachari, K.; Foresman, J. B.; Ortiz, J. V.; Cui, Q.; Baboul, A. G.; Clifford, S.; Cioslowski, J.; Stefanov, B. B.; Liu, G.; Liashenko, A.; Piskorz, P.; Komaromi, I.; Martin, R. L.; Fox, D. J.; Keith, T.; Al-Laham, M. A.; Peng, C. Y.; Nanayakkara, A.; Challacombe, M.; Gill, P. M. W.; Johnson, B.; Chen, W.; Wong, M. W.; Gonzalez, C.; Pople, J. A. *Gaussian 03*, Revision C.02; Gaussian, Inc.: Wallingford, CT, 2004.
- (70) van der Spoel, D.; Lindahl, E.; Hess, B.; Groenhof, G.; Mark, A. E.; Berendsen, H. J. C. GROMACS: Fast, Flexible, and Free. *J. Comput. Chem.* **2005**, *26*, 1701.
- (71) Hess, B.; Kutzner, C.; van der Spoel, D.; Lindahl, E. GROMACS 4: Algorithms for Highly Efficient, Load-Balanced, and Scalable Molecular Simulation. *J. Chem. Theory Comput.* **2008**, *4*, 435.
- (72) NIST Chemistry WebBook. <http://webbook.nist.gov/chemistry> (accessed June 2011).
- (73) Nosé, S. A Molecular Dynamics Method for Simulations in the Canonical Ensemble. *Mol. Phys.* **1984**, *52*, 255.
- (74) Hoover, W. G. Canonical Dynamics: Equilibrium Phase-Space Distributions. *Phys. Rev. A* **1985**, *31*, 1695.
- (75) Parrinello, M.; Rahman, A. Polymorphic Transitions in Single Crystals: A New Molecular Dynamics Method. *J. Appl. Phys.* **1981**, *52*, 7182.
- (76) Nosé, S.; Klein, M. L. Constant Pressure Molecular Dynamics for Molecular Systems. *Mol. Phys.* **1983**, *50*, 1055.
- (77) Essman, U.; Perera, L.; Berkowitz, M. L.; Darden, T.; Lee, H.; Pedersen, L. G. A Smooth Particle Mesh Ewald Method. *J. Chem. Phys.* **1995**, *103*, 8577.
- (78) Hess, B.; Bekker, H.; Berendsen, H. J. C.; Fraaije, J. G. E. M. LINCS: A Linear Constraint Solver for Molecular Simulations. *J. Comput. Chem.* **1997**, *18*, 1463.
- (79) Hess, B. P-LINCS: A Parallel Linear Constraint Solver for Molecular Simulation. *J. Chem. Theory Comput.* **2008**, *4*, 116.
- (80) Allen, M. P.; Tildesley, D. J. *Computer simulation of liquid*; Clarendon Press: Oxford, U. K., 1987.
- (81) Kohlrausch, F. Ueber die elastische Nachwirkung bei der Torsion. *Ann. Phys.* **1863**, *119*, 337.
- (82) Williams, G.; Watts, D. C. Non-Symmetrical Dielectric Relaxation Behaviour Arising from a Simple Empirical Decay Function. *Trans. Faraday Soc.* **1970**, *66*, 80.
- (83) Hess, B. Determining the Shear Viscosity of Model Liquids from Molecular Dynamics Simulations. *J. Chem. Phys.* **2002**, *116*, 209.
- (84) Wensink, E. J. W.; Hoffmann, A. C.; van Maaren, P. J.; van der Spoel, D. Dynamic Properties of Water/Alcohol Mixtures Studied by Computer Simulation. *J. Chem. Phys.* **2003**, *119*, 7308.
- (85) Berendsen, H. J. C.; Postma, J. P. M.; DiNola, A.; Haak, J. R. Molecular Dynamics with Coupling to an External Bath. *J. Chem. Phys.* **1984**, *81*, 3684.
- (86) Wang, J.; Cieplak, P.; Kollman, P. A. How Well Does a Restrained Electrostatic Potential (RESP) Model Perform in Calculating Conformational Energies of Organic and Biological Molecules? *J. Comput. Chem.* **2000**, *21*, 1049.
- (87) Grolier, J.-P. E.; Roux-Desgranges, G.; Berkane, M.; Jiménez, E.; Wilhelm, E. Heat Capacities and Densities of Mixtures of very Polar Substances 2. Mixtures containing *N,N*-dimethylformamide. *J. Chem. Thermodynamics* **1993**, *25*, 41.
- (88) Dymond, J. H.; Robertson, J.; Isdale, J. D. Transport Properties of Nonelectrolyte Liquid Mixtures — IV. Viscosity Coefficients for Benzene, Perdeuterobenzene, Hexafluorobenzene, and an Equimolar Mixture of Benzene + Hexafluorobenzene from 25 to 100 °C at Pressures up to the Freezing Pressure. *Int. J. Thermophys.* **1981**, *2*, 223.
- (89) McCool, M. A.; Collings, A. F.; Woolf, L. A. Pressure and Temperature Dependence of the Self-Diffusion of Benzene. *J. Chem. Soc., Faraday Trans. 1* **1972**, *68*, 1489.
- (90) Witt, R.; Sturz, L.; Dölle, A.; Müller-Plathe, F. Molecular Dynamics of Benzene in Neat Liquid and a Solution Containing Polystyrene. <sup>13</sup>C Nuclear Magnetic Relaxation and Molecular Dynamics Simulation Results. *J. Phys. Chem. A* **2000**, *104*, 5716.
- (91) Alper, H. E.; Bassolino, D.; Stouch, T. R. Computer Simulation of a Phospholipid Monolayer-Water System: The Influence of Long Range Forces on Water Structure and Dynamics. *J. Chem. Phys.* **1993**, *98*, 9798.
- (92) Alper, H. E.; Bassolino-Klimas, D.; Stouch, T. R. The Limiting Behavior of Water Hydrating a Phospholipid Monolayer: A Computer Simulation Study. *J. Chem. Phys.* **1993**, *99*, 5547.